Cell

A Landmark Protein Essential for Establishing and Perpetuating the Polarity of a Bacterial Cell

Hubert Lam,[1] Whitman B. Schofield,[1] and Christine Jacobs-Wagner[1,*]
[1] Department of Molecular, Cellular, and Developmental Biology, Yale University, New Haven, CT 06520, USA
*Contact: christine.jacobs-wagner@yale.edu
DOI 10.1016/j.cell.2005.12.040

SUMMARY

Polarity is often an intrinsic property of the cell, yet little is known about its origin or its maintenance over generations. Here we identify a landmark protein, TipN, which acts as a spatial and temporal cue for setting up the correct polarity in the bacterium *Caulobacter crescentus*. TipN marks the new pole throughout most of the cell cycle, and its relocation to the nascent poles at the end of division provides a preexisting reference point for orienting the polarity axis in the progeny. Deletion of *tipN* causes pleiotropic polarity defects, including frequently reversed asymmetry in progeny size and mislocalization of proteins and organelles. Ectopic localization of TipN along the lateral side of the cell creates new axes of polarity leading to cell branching and formation of competent cell poles. Localization defects of the actin-like protein MreB in the Δ*tipN* mutant suggest that TipN is upstream of MreB in regulating cell polarity.

INTRODUCTION

Cell polarity is one of the most basic principles of biology as most cells rely on cell polarization for processes as diverse as growth, division, morphogenesis, and migration. While the origin of cell polarization is poorly understood, it is believed that the orientation of the chosen polarity axis is defined by an intracellular asymmetry. This positional information can be generated by an extracellular cue provided by the environment, for example during chemotaxis and cell migration. However, in many cases, cell polarity originates from no external cue and appears to constitute an inherent property of the cell. How cell polarity is intrinsically acquired remains largely unclear.

The dimorphic bacterium *Caulobacter crescentus* provides a valuable, single-cell model system to probe the basic mechanisms of inherent cell polarity. In this crescent-shaped organism, cell polarity is intrinsically acquired and is morphologically apparent by the formation of polar appendages and by the asymmetric division that generates progeny of unequal size. These morphological manifestations of cell polarity are faithfully reproduced during each cell cycle and are essential for the life cycle of this organism (Figure 1). *C. crescentus* exists in two cell types: a motile, DNA replication-quiescent "swarmer cell" and a sessile, DNA replication-competent "stalked cell"; the former is important for dispersion and the latter for reproduction. During the cell cycle (Figure 1), the swarmer cell, which has a single flagellum and several pili at one cell pole, grows into a stalked cell. During this swarmer-to-stalked cell transition, the flagellum and pili are lost, and a stalk, a thin extension of the cell body, elongates at the pole originally occupied by the flagellum. The stalked cell then initiates chromosome replication and cell division. During the predivisional stage, a new flagellum and a pilus secretion apparatus are assembled specifically at the stalk-distal pole. This results in a morphologically asymmetric predivisional cell with a flagellum at one pole and a stalk at the other. The cell cycle ends with an asymmetric cell division producing a shorter swarmer cell and a longer stalked cell. To compensate for this cell size asymmetry, the stalked daughter cell skips the period of growth that occurs during the development of the swarmer daughter cell into a stalked cell (Figure 1).

The polarity axis, which spans between the "new pole" created at the previous division and the "old pole" originating from an earlier division, is readily apparent in *C. crescentus* by the targeting of flagellar and pilus proteins to the new pole, the formation of the stalk at the old pole, and the polarization of the cell division apparatus toward the new pole to create a swarmer progeny smaller than its stalked sibling (Figure 1). With each division, the identity of the poles (new versus old) must be redefined to restore the polarity axis in the stalked progeny and to reverse it in the swarmer progeny (Figure 1). The mechanism by which this occurs is unknown.

It was recently proposed that the bacterial actin homolog, MreB, is involved in generating cell polarity in *C. crescentus* and *Escherichia coli* (Gitai et al., 2004; Nilsen et al., 2005; Shih et al., 2005; Wagner et al., 2005). In *C. crescentus*, MreB exhibits a dynamic organization during the cell cycle, which alternates between a spiral-like structure along the polarity axis and a ring-like structure at the

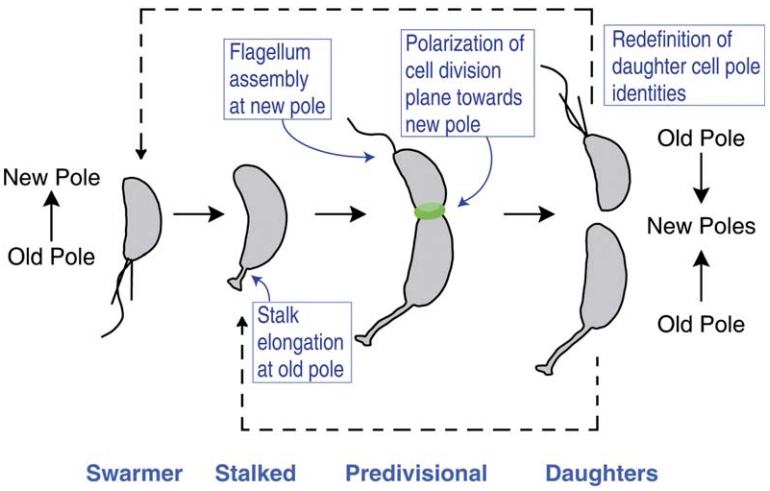

Figure 1. Morphological Manifestations of Cell Polarity during the Cell Cycle of *C. crescentus*

Morphogenesis and division during the *C. crescentus* cell cycle rely on a polarity axis defined by the identity of the two cell poles. The newborn swarmer cell grows and differentiates into a stalked cell by losing its polar flagellum and pili and growing a stalk at the old cell pole. At the predivisional cell stage, the cell assembles a new flagellum at the new pole, and the division plane (in green) is laid down at a distance closer to the new pole than the old one. The polarization of division along the polarity axis results in generation of two daughter cells of unequal size, a shorter swarmer cell and a longer stalked cell. The creation of new poles by division redefines the pole identities in the daughter cells and re-establishes the polarity axis in the stalked progeny while reversing it in the swarmer progeny. To compensate for the size asymmetry, the swarmer progeny grows before becoming a stalked cell whereas the stalked progeny skips this period of growth.

division plane (Figge et al., 2004; Gitai et al., 2004). MreB-depleted cells lose cell polarity as well as the characteristic crescent shape of *C. crescentus* to adopt a more spherical morphology, presumably by switching to an isotropic mode of growth (Figge et al., 2004; Gitai et al., 2004). Restoration of MreB synthesis in these spheroid cells reestablishes polarization, although often with the wrong polarity (Gitai et al., 2004; Wagner et al., 2005). Other factors acting on the regulation of cell polarity have remained elusive.

Here we describe the identification of a cell polarity determinant responsible for setting up the proper polarity of the cell by providing a positional cue from the preceding division cycle.

RESULTS

A Coiled-Coil Rich Protein, TipN, Marks the New Pole of the Cell

The budding yeast *Saccharomyces cerevisiae*, a well-studied eukaryotic model for cell polarity, can use previous division sites as spatial cues to specify new cell polarity sites (Chant and Pringle, 1995). In *C. crescentus*, the site of the most recent division is the new pole. Thus, by analogy to the yeast system, we postulated that a protein or a protein complex involved in establishing bacterial cell polarity would be localized at the new pole to create cellular asymmetry. We further speculated that such a polarizing complex, if present, may include anchor or scaffolding proteins with transmembrane regions for membrane attachment and large protein interaction domains, such as coiled-coils, to mediate or stabilize interactions within the polar complex. Using this last assumption to search the *C. crescentus* genome, we identified several candidates including gene *CC1485*, which encodes an uncharacterized, 888 residue protein (accession number AAK23464) with two transmembrane-spanning segments and a large portion of its amino-acid sequence in coiled-coil conformation based on predictive algorithms (Figure 2A). This protein, now renamed TipN (*Tip* of *N*ew pole), was found to localize at the tip of the new pole or nascent poles created by division. This was demonstrated in timelapse and timecourse fluorescence microscopy experiments on synchronized cell-cycle populations using a *tipN-gfp* fusion in place of *tipN* at the chromosomal locus (strain CJW1406) (Figures 2B and S1A; Movie S1). In the newborn swarmer cell, TipN-GFP was localized at the new pole and remained there for most of the cell cycle. The new pole was identified by the formation of the stalk, an old-pole marker, at the opposite pole. At the late predivisional stage, the TipN-GFP signal disappeared from the pole to reappear at the division site after a brief period of fairly diffuse distribution. This change in localization to the division site resulted in daughter cells with TipN-GFP at their new pole after cell separation.

Immunoblot analysis of synchronized CJW1406 cell-cycle extracts revealed that TipN-GFP was present at similar levels throughout the cell cycle (Figure 2C; MreB served as a loading control). No degradation was apparent at the 75 min time point when TipN-GFP changed locations (as examined in parallel by microscopy). The quality of the synchrony was attested to by the cell cycle-dependent pattern of CtrA (Domian et al., 1997). Similarly, the levels of TipN remained constant throughout the cell cycle of wild-type CB15N cells (Figure S1B). Moreover, pulse-chase experiments after [^{35}S]Met labeling indicated that TipN-GFP was very stable relative to the length of the cell cycle (2 hr under these conditions), as no significant degradation was observed over a period of 3.5 hr (data not shown). Thus, the change in TipN-GFP localization at the end of division does not seem to be the result of specific degradation or de novo synthesis; instead the results argue for the movement of TipN-GFP from the pole to the division site.

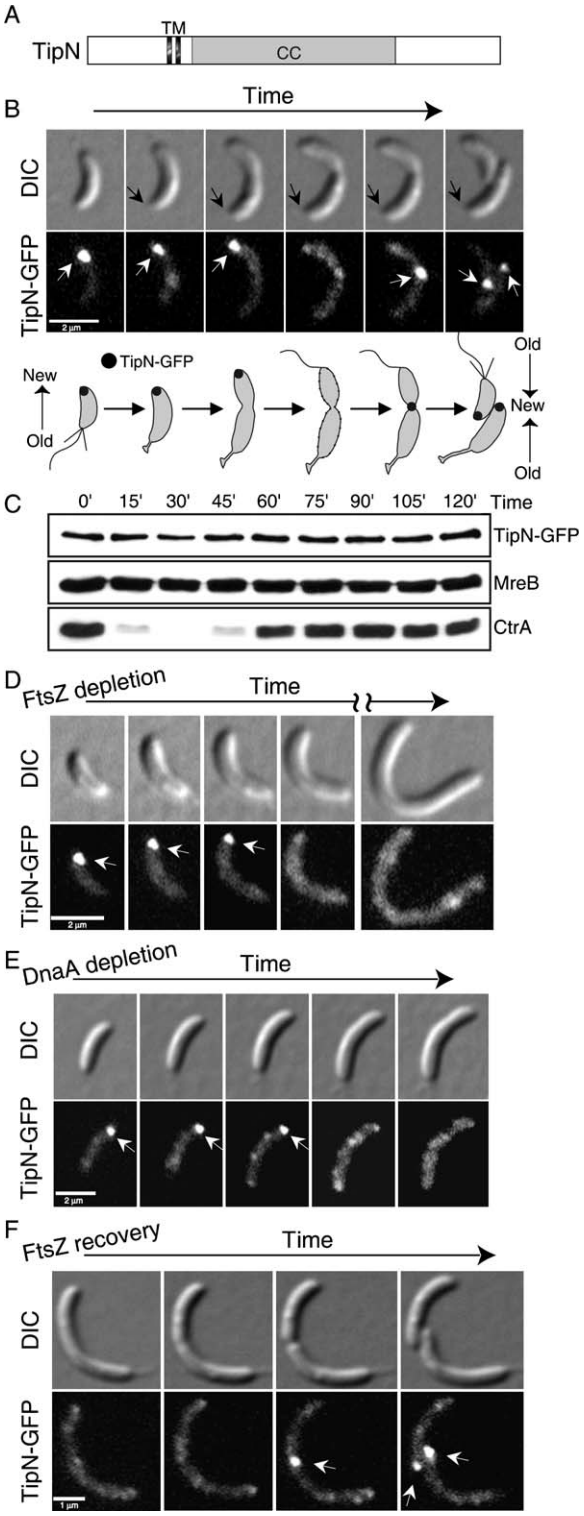

Figure 2. TipN Is a Membrane Bound Coiled-Coil-Rich Protein that Marks the New or Nascent Poles of *C. crescentus* during the Cell Cycle

Black and white arrows indicate stalks and TipN-GFP foci, respectively.

The polar delocalization of TipN-GFP and its relocation to division sites always occurred at the late predivisional stage, irrespective of growth rates and cell-cycle lengths (as analyzed by varying growth media and temperature), suggesting that this dynamic sequence may be controlled by cell-cycle events. However, TipN-GFP was, remarkably, still released from the new pole even when initiation of cell division or DNA replication was inhibited. Swarmer cells carrying *ftsZ* or *dnaA* under a xylose-inducible promoter were isolated from cultures containing xylose (0.3%) and were spotted onto an agarose-padded slide lacking xylose, which turned off *ftsZ* or *dnaA* expression and effectively prevented initiation of cell division or DNA replication (Gorbatyuk and Marczynski, 2001; Wang et al., 2001). Under these conditions, TipN-GFP retained its normal localization at the new pole during cell elongation and was released from the pole when the cells reached the size characteristic of the late predivisional stage despite the absence of division (Figure 2D) or DNA replication (Figure 2E; DnaA-depleted cells also failed to divide because of the known dependency of cell division on DNA replication). TipN-GFP levels were similar before and after its delocalization from the new pole under both FtsZ and DnaA depletion conditions, consistent with the notion of TipN-GFP movement rather than proteolysis (data not shown). Thus, the polar delocalization of TipN-GFP does not require the completion of a cell division event or a DNA replication or DNA segregation step since none of these events can occur in the absence of initiation of division or DNA replication. Similarly, flagellar rotation or

(A) Illustration depicting the domain architecture of TipN. TipN contains two predicted transmembrane-spanning segments (TM) and a large coiled-coil region (CC).

(B) TipN-GFP localizes at the new or nascent cell poles during the cell cycle. The localization of TipN-GFP in strain CJW1406 was monitored during the cell cycle by timelapse microscopy starting with a synchronous population of swarmer cells.

(C) Western blot analysis of relative TipN-GFP protein levels during the cell cycle starting with a synchronous population of swarmer CJW1406 cells. MreB and CtrA proteins are shown as loading control and quality control for the synchrony, respectively.

(D) Inhibition of cell division by FtsZ depletion still permits release of TipN-GFP from the new pole but prohibits relocalization to the potential division sites. Swarmer cells were isolated from a CJW1487 cell population grown in M2G$^+$ supplemented with 0.3% xylose and spotted on an M2G$^+$ agarose pad containing 0.2% glucose for timelapse microscopy of TipN-GFP during FtsZ depletion.

(E) Inhibition of initiation of DNA replication by turning off *dnaA* expression also permits release of TipN-GFP from the new pole. Swarmer cells carrying *dnaA* under xylose-inducible expression (CJW1482) grown in the presence of 0.3% xylose were isolated and spotted on an M2G$^+$ agarose pad supplemented with 0.2% glucose for timelapse microscopy of TipN-GFP.

(F) Restoration of cell division in elongated FtsZ-depleted cells by reinducing *ftsZ* expression causes relocalization of TipN-GFP at division sites. Swarmer CJW1487 cells were depleted of FtsZ (as in D), thereby inhibiting initiation of cell division. After 120 min of elongation under these conditions, the cells were washed and examined by timelapse microscopy on M2G$^+$ agarose pad containing 0.3% xylose that restored *ftsZ* expression and cell division.

flagellum and pilus synthesis cannot be involved in triggering TipN-GFP delocalization since these morphogenetic events are also prevented by blocking either cell division or DNA replication (Ohta and Newton, 1996). Instead, the fact that the polar release of TipN-GFP occurred at a similar cell length in wild-type (4.10 ± 0.45 μm; n = 50), FtsZ-depleted (4.11 ± 0.51 μm; n = 50), and DnaA-depleted cells (4.04 ± 0.70 μm; n = 72) suggests that this step is controlled by cell size.

Unlike its polar release, the relocation of TipN-GFP to the division site was controlled by cell division, as TipN-GFP was unable to accumulate at potential division sites in FtsZ-depleted cells (and DnaA-depleted cells by virtue of the division block) (Figures 2D and 2E). When cell division was restored to FtsZ-depleted cells by addition of xylose, TipN-GFP molecules were recruited to the division sites, yielding two daughter cells with TipN-GFP at the correct, new pole (Figure 2F). TipN-GFP levels were similar before and after restoration of cell division (data not shown).

Altogether, our results indicate that progeny cells inherit TipN-GFP at their new pole from the previous division cycle in a two-step mechanism that appears to depend on cell size and cell division.

A *tipN* Null Mutant Exhibits Multiple Cell Polarity Defects

The localization pattern of TipN-GFP during the cell cycle raised the possibility that TipN provides a positional cue at the new pole, perhaps important for establishing cell polarity. To investigate this possibility, we created a deletion of *tipN*. The resulting Δ*tipN* strain exhibited a minor growth defect as compared to the wild-type strain (CB15N) in PYE medium at 30°C (with a doubling time of 93 ± 5 min and 99 ± 5 min for CB15N and Δ*tipN*, respectively). Importantly, microscopic analysis revealed that Δ*tipN* caused several cell polarity defects, as described below.

In wild-type cells, the division plane is polarized toward the new pole, yielding a swarmer daughter cell shorter than its stalked sibling (Terrana and Newton, 1975). In striking contrast, Δ*tipN* cells often exhibited an apparent reversed asymmetry with swarmer cells being longer than their stalked siblings as shown by electron microscopy (EM) of late predivisional cells (Figure 3A) and by timelapse differential interference contrast (DIC) microscopy of dividing cells (Figure 3B and Movie S2, both showing two division cycles). This reversed asymmetry in progeny size suggested a mispolarization of the division plane. An alternative interpretation, however, is that the stalk, used here as a morphological marker to identify the old pole, was placed at the wrong pole (i.e., new pole), leading to confusion about the identity of the two daughter cells. This alternative was ruled out by examining the subcellular distribution of the DNA replication inhibitor CtrA, which identifies the daughter cells based on their competence for DNA replication (Domian et al., 1997; Judd et al., 2003). In both wild-type and Δ*tipN* late predivisional cells, a YFP-CtrA fusion was absent from the stalked compartment to permit initiation of DNA replication there, whereas YFP-CtrA was present in the swarmer compartment where it represses DNA replication (data not shown). Thus, the location of the stalk in Δ*tipN* cells could be used to identify the old pole and the replication-competent progeny. This implied that the progeny size, and thus the polarization of the division machinery, was often reversed in the absence of TipN. To determine the frequency of this abnormality, we measured the length between each pole and the site of division in late predivisional cells using the stalk as an old-pole marker. As expected, in wild-type cells the stalked compartment was longer than the swarmer compartment (mean ratio of 1.20 ± 0.15; n = 128). In contrast, only 34% of Δ*tipN* cells had a normal stalked-to-swarmer compartment length ratio (>1), whereas the remaining 66% had a stalked compartment smaller than the swarmer compartment (overall mean ratio of this mixed population was 0.94 ± 0.31; n = 307; a paired t test of the wild-type versus Δ*tipN* data set gave a p value less than 0.0001). Normal bias in progeny size was restored in Δ*tipN* cells by trans-complementation with *tipN-gfp* (data not shown).

The correct polarization, and thus placement, of the division plane is critical for maintaining the characteristic cell lengths for each cell-cycle stage. The normal bias of the division plane location toward the new pole produces a swarmer cell that is shorter than its stalked cell sibling; growth of the swarmer cell during its transition to the stalked cell stage compensates for this difference (Figure 1). However, when this bias is reversed, as we often observed in the Δ*tipN* population, division yields a swarmer cell longer than its stalked sibling. Growth of this swarmer cell, normally responsible for length equalization, leads to a progressive lengthening of the swarmer cell and the stalked cell into which it develops. This cell size problem is exacerbated by increasing numbers of consecutive mispolarized divisions (see example in Figure 3B and Movie S2), contributing to the high proportion of elongated cells in the Δ*tipN* population (31%, n = 1051) (Figure S2A). Furthermore, analysis of DIC images revealed that approximately 3% of Δ*tipN* cells (n = 1091) had a division plane near a pole, thus forming a minicell (the formation of these minicells was also apparent in EM images; Figure S2B). Since all cells, dividing and nondividing, were counted, this percentage represents an underestimation of the minicelling phenotype, providing further evidence of misregulation of the division plane placement. Thus, TipN is required for the correct placement of the division plane along the polarity axis of the cell.

Since the Δ*tipN* mutation impaired the proper polarization of the division machinery, we next investigated whether localization of polar organelles was perturbed in the absence of TipN. This was particularly relevant for the flagellum, which normally assembles at the new pole where TipN localizes. To visualize flagella, we developed a convenient fluorescence method that uses cell fixation and DAPI stain (see Experimental Procedures). Figure 3C shows such DAPI staining of wild-type predivisional cells with a flagellum at the new pole. In Δ*tipN* mutant cells,

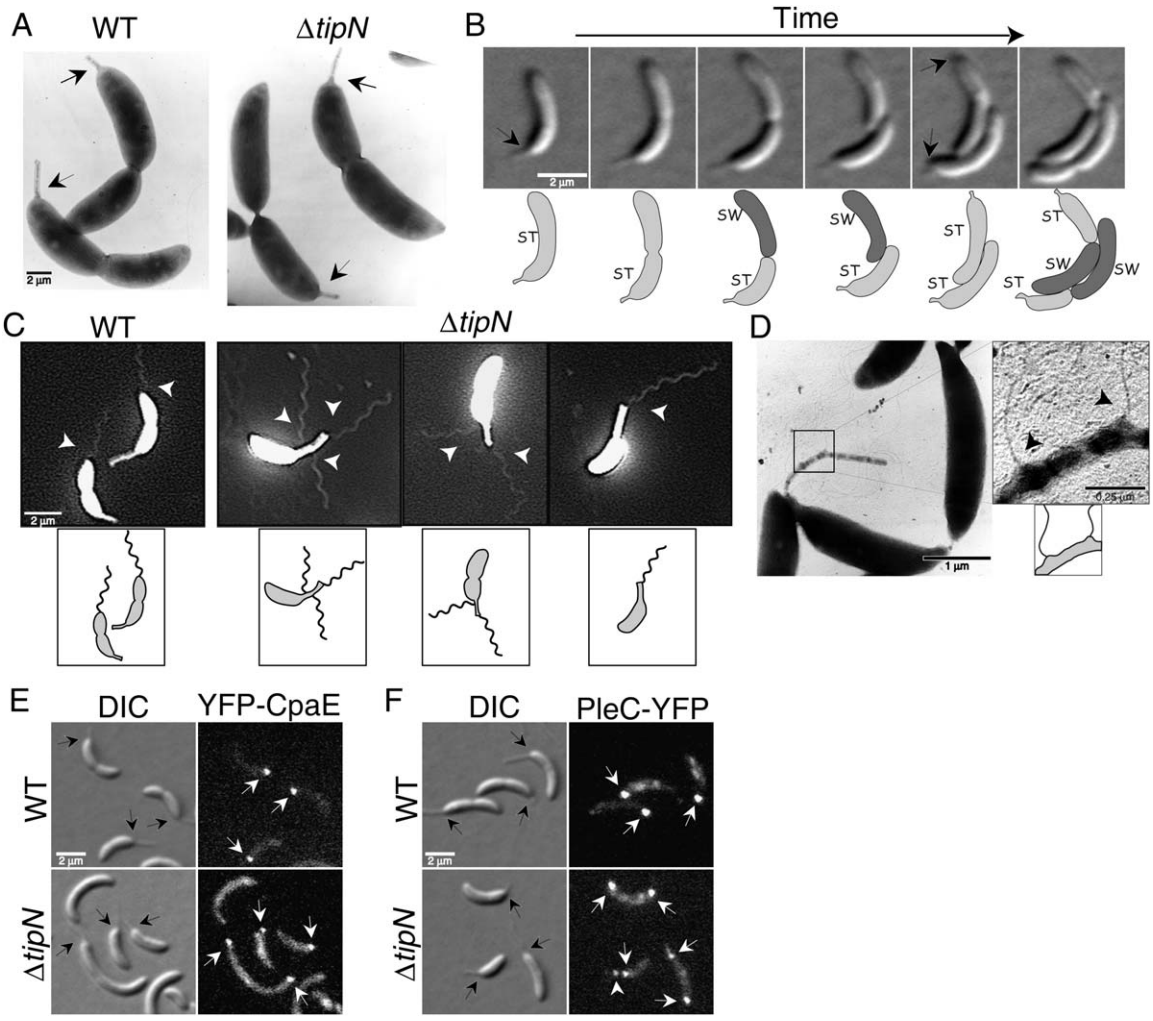

Figure 3. A *tipN* Null Mutant Exhibits Pleiotropic Cell Polarity Defects

(A) Electron micrographs of wild-type (CB15N) and Δ*tipN* (CJW1407) predivisional cells. In wild-type cells, the polarization of the division plane toward the new pole is responsible for the generation of a swarmer cell that is shorter than its stalked sibling after division. In Δ*tipN* cells, the division plane is often mispolarized toward the old pole, which ultimately leads to a reversed asymmetry in daughter cell size. Black arrows show the stalk, identifying the old pole.

(B) Timelapse DIC microscopy of a Δ*tipN* mutant cell illustrating the frequent reversed polarization of division in the absence of TipN, which results in a swarmer cell (SW) that is longer than its stalked sibling (ST). Consecutive mispolarized divisions cause a lengthening of the swarmer cell and an increased discordance between the cell length and the cell cycle stage. Black arrows show the location of the stalk.

(C) The placement of the flagellum is often incorrect in Δ*tipN* cells. Flagellar staining shows that the flagellum is located at the new pole of wild-type predivisional cells. In the absence of TipN, one or several flagella are often found emerging from the wrong location such as the stalked pole or the stalk itself. Arrowheads point to the flagella. A schematic is shown below.

(D) Electron micrograph of Δ*tipN* cells showing two flagella protruding from the lateral side of a stalk. The boxed region on the right panel is shown at a higher magnification with a schematic shown below. Flagella are indicated by arrowheads.

(E) The localization of the pilus secretion protein CpaE is often perturbed in the absence of TipN. When TipN is present (strain PV418), YFP-CpaE localizes at the new pole of predivisional cells, opposite the stalk. In the absence of TipN (CJW1421), however, YFP-CpaE is regularly localized at the wrong, stalked pole or at both poles. Black and white arrows indicate the stalks and YFP-CpaE foci, respectively.

(F) Correct localization of the histidine kinase PleC at the new pole requires TipN. In a wild-type background (LS3205), a PleC-YFP fusion forms a single fluorescent focus at the new pole of predivisional cells. In contrast, PleC-YFP is often misplaced at the old, stalked pole (occasionally within the stalk itself; white arrowhead) or at both poles in a Δ*tipN* background (CJW1410). Black and white arrows indicate the stalks and PleC-YFP foci, respectively.

the location of the flagellum was often incorrect with 76% of predivisional cells possessing a flagellum at the wrong, old pole and only 24% at the correct, new pole (n = 85). When the flagellum was mislocalized at the old pole, it often appeared to come out of the side or (close to) the tip of the stalk (Figure 3C); this was confirmed by EM (Figure 3D). Emergence of a flagellum from the side of a stalk suggested that, in some Δ*tipN* cells, the flagellum assembly

occurred at the old pole next to a nascent stalk and that the flagellum was incorporated into the stalk during its growth. Since the stalk is a thin extension of the cell body that continues to elongate in progressive cell cycles, this event could occur more than once, resulting in stalks decorated with several flagella (Figures 3C and 3D). The defects in flagella positioning due to a loss of TipN function were accompanied by a reduced motility as determined by swarm assay (data not shown).

The spatial regulation of the pilus secretion machinery was also perturbed in the absence of TipN. This was shown by looking at the localization of a YFP fusion to CpaE, a component of the pilus secretion machinery, which forms a weak fluorescent focus at the new pole of predivisional cells where pili assemble after division (Viollier et al., 2002). We found that, as expected, YFP-CpaE targeting at the new pole of wild-type predivisional cells was very precise with no mislocalization of YFP-CpaE at the stalked (old) pole (n = 137) (Figure 3E). However, in the Δ*tipN* background, YFP-CpaE localization was more variable with 57% mislocalized either at the stalked pole or at both poles (30% and 27%, respectively) and only 43% correctly localized at the new pole (n = 409) (Figure 3E). This suggests that TipN is required for faithful assembly of the pilus secretion apparatus at the correct pole. Although the positioning of the stalk at the correct, old pole for the most part did not require TipN, 3% of Δ*tipN* cells (counting all cell types, which implied an underestimation of the defect; n = 1091) had bipolar stalks (Figure S2C). While this is significant, the loss of TipN function appears to most dramatically affect the spatial regulation of organelles that assemble at the new pole.

To assess whether TipN also affects the spatial regulation of other proteins known to polarly localize, we examined the distribution of DivJ and PleC, two histidine kinases known to localize at opposite poles in predivisional cells (Wheeler and Shapiro, 1999). As expected, in a wild-type background, predivisional cells exhibited a robust localization of PleC-YFP and DivJ-CFP at the new and old poles, respectively. Mislocalization of PleC-YFP and DivJ-CFP was only rarely observed when TipN was present (<1%; n = 105). While DivJ-CFP localization at the old (stalked) pole was normal in a Δ*tipN* background (data not shown), the location of PleC-YFP, on the other hand, was variable (Figure 3F). In these cells, PleC-YFP could be found at the new pole (36%), old (stalked) pole (19%), or both poles (45%) (n = 139). Interestingly, PleC-YFP foci were occasionally present within the actual stalk of Δ*tipN* cells (Figure 3F; white arrowhead), reminiscent of the stalk-based origin of some flagella in Δ*tipN* cells.

Altogether, our results are consistent with a distortion of cell polarity when TipN function is lost. The most dramatic effect was the frequent reversed polarity in Δ*tipN* cells as manifested by the reversed asymmetry in progeny size and the mislocalization of new-pole-specific organelles and proteins to the wrong (old) pole. This strongly suggests that TipN plays a crucial role in orienting the polarity axis of the cell.

Perturbed Localization of TipN Affects Flagellar Placement

TipN-GFP localizes at the new pole for most of the cell cycle until the late predivisional stage at which time TipN-GFP loses its polar localization to reappear at the site of cell division where new poles are being formed (Figure 2B). However, under mild overproduction conditions by expression in wild-type CB15N from a low-copy plasmid (pMR20; ~2–5 copies), TipN-GFP regularly failed to lose its polar localization at the late predivisional stage while still forming a focus at the site of cell division, generating a bipolar localization of TipN-GFP in many swarmer progeny (Figure S3A). The normal localization of TipN-GFP at the new pole only was restored at a later time point in the swarmer cell stage. Thus, mild overproduction of TipN-GFP caused a transient bipolar localization of TipN-GFP in the beginning of the swarmer cell-cycle stage, which, in turn, appeared to affect flagellum placement. Sixty-seven percent of predivisional cells with plasmid-encoded TipN (n = 137) had a flagellum emerging from the stalked (old) pole or from the stalk itself (Figures S3B and S3C).

Ectopic Localization of TipN along the Lateral Sides of the Cell Results in New Growth Sites and Formation of New Poles

Since localization of TipN appears important for TipN function, we reasoned that ectopic localization of TipN caused by overproduction might create new axes of polarity. To test this hypothesis, *tipN-gfp* was placed under the control of the xylose-inducible promoter on a low-copy plasmid (pMR20PxyltipN-gfp) in an otherwise wild-type background. Overexpression of *tipN-gfp* by xylose induction for 18 hr resulted in elongated and branched cells with TipN-GFP forming foci not only at the poles of the cell but also at the leading edge of every branch (Figure 4A). The *tipN-gfp*-overexpressing cell population also consisted of cells with bumps along their cell length or cells with large, bifurcated poles. In each case, TipN-GFP marked these errant growth sites (Figure 4A), suggesting that these morphological abnormalities were sites of future branches and that ectopic localization of TipN-GFP redirected cell growth at these branch sites.

Timelapse microscopy experiments confirmed that ectopic TipN was the cause and not a consequence of the branching phenotype, as ectopic localization of TipN-GFP along the lateral side of a cell preceded the formation of a branch (Figure 4B; Movie S3). Thus, ectopic TipN specified sites of branch emergence. Not surprisingly, the presence of TipN-GFP at several locations within the cell caused mispolarization of the division plane as evidenced by filamentation (Figure 4A) and production of minicells (Figure 4B, yellow arrowheads; Movie S3).

Normally, cell poles are only the products of cell division. However, ectopic TipN induced the formation of poles at the end of branches that resembled in size and appearance those formed by division (Figure 4A). These branch poles were recognized by the cell as bona fide poles, as

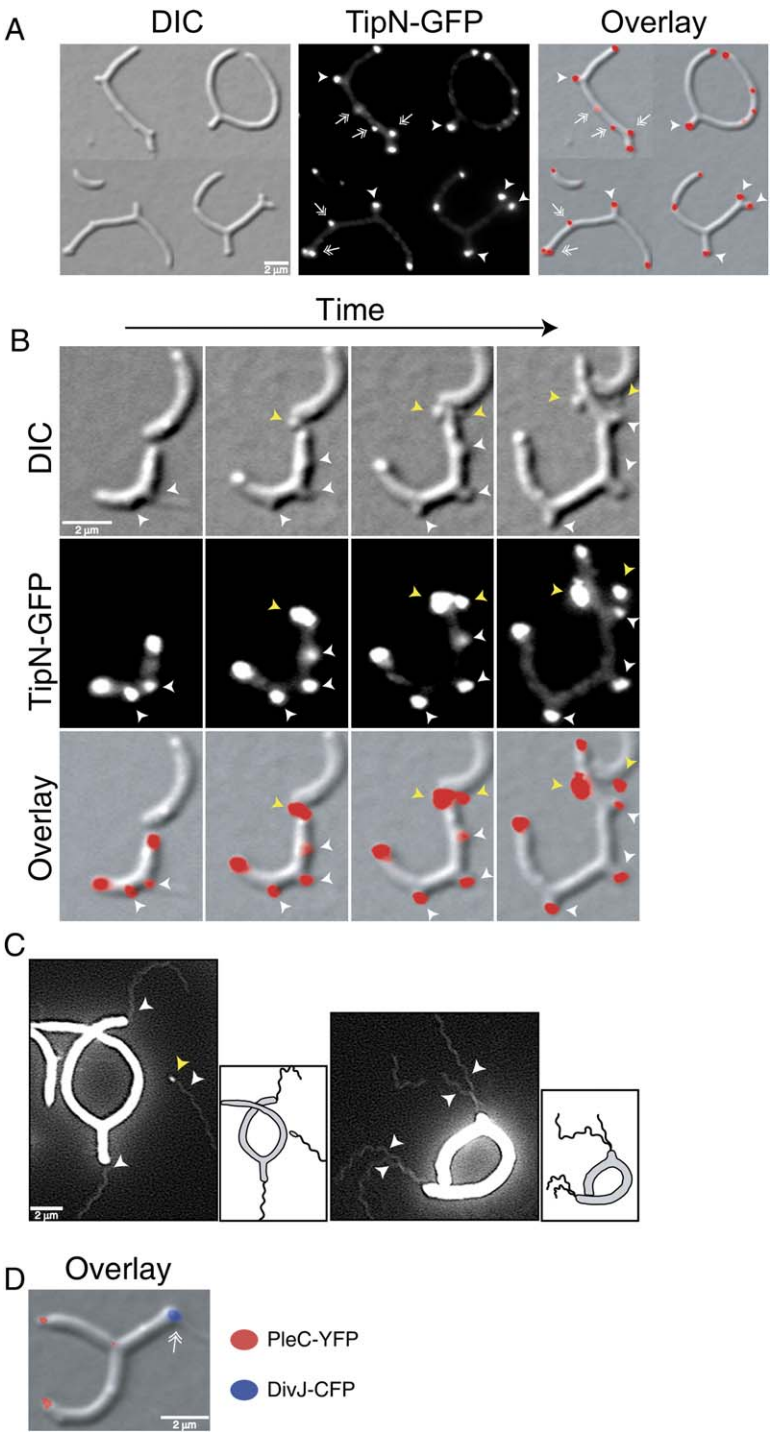

Figure 4. Ectopic Localization of TipN Results in a New Axis of Cell Growth and in Formation of a Competent Pole

(A) Induction of *tipN-gfp* expression with 0.3% xylose for 18 hr in PYE causes cell elongation and branching of CJW1414. TipN-GFP was found ectopically localized at the leading edge of cell branches (arrowheads) and at pre-branch sites (hatched arrows), which appeared as bumps along the cell surface.

(B) Timelapse microscopy of cells overexpressing *tipN-gfp* indicates that ectopic localization of TipN-GFP is the cause of the branching phenotype as the localization of TipN-GFP along the lateral side of the cell precedes the formation of an ectopic pole (white arrowheads). CJW1414 cells were grown in M2G^{+} in the presence of 0.3% xylose for 10 hr before being mounted on an agarose-padded slide containing M2G^{+}, but no xylose. DIC and fluorescent images were taken at regular intervals for a total of 360 min. Yellow arrowheads show formation of two minicells.

(C) Overproduction of TipN results in formation of new poles competent for flagellar assembly. CJW1413 cells were grown in PYE in the presence of 0.3% xylose for 18 hr before DAPI staining. White and yellow arrowheads show flagella and a flagellated minicell, respectively. A schematic representation is displayed to the right of the fluorescence image.

(D) Overproduction of TipN results in formation of poles competent for protein localization. Cells (CJW1452) coexpressing *pleC-yfp* and *divJ-cfp* and carrying pMR20PxyltipN were grown in PYE in the presence of 0.3% xylose for 18 hr before imaging. DIC and fluorescent images were overlaid to show the polar localization of PleC-YFP (red) and DivJ-CFP (blue). The stalk is indicated by a hatched arrow.

they were fully competent for flagellar assembly and localization of proteins normally found at the pole (Figures 4C and 4D).

These observations are consistent with TipN specifying new sites of cell polarity, with ectopic localization resulting in cell branching and formation of new poles.

Proper Localization of MreB Requires TipN Function

Since the actin homolog MreB is thought to play an important role in cell polarization in *C. crescentus* (Gitai et al., 2004; Wagner et al., 2005), we next tested whether MreB affected TipN localization and vice versa. Cells expressing *tipN-gfp* (CJW1406) were exposed to A22, a chemical that

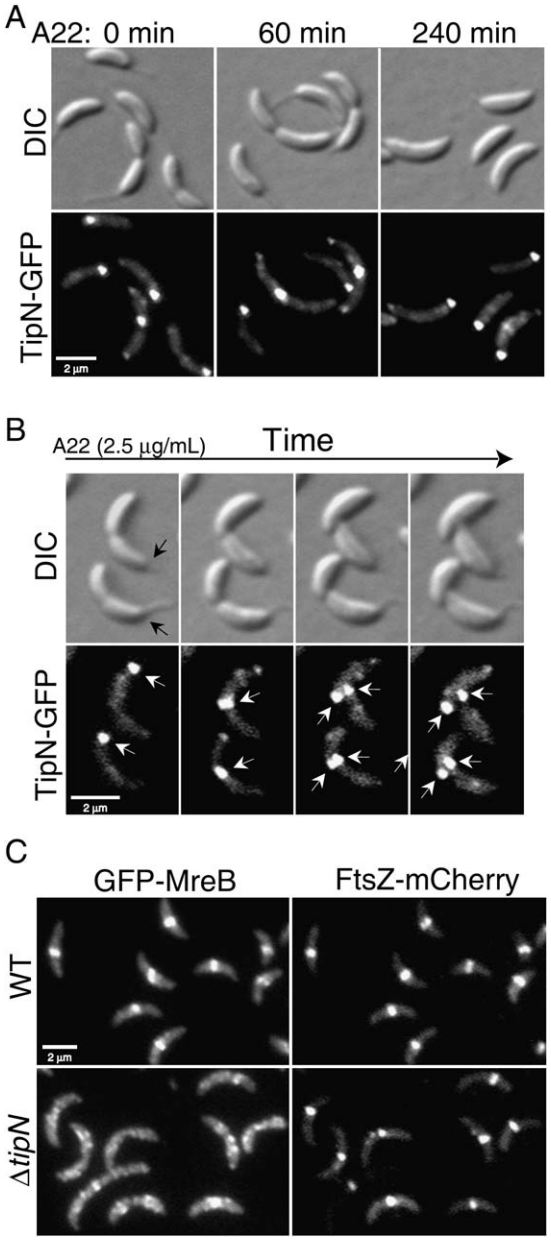

Figure 5. TipN Is Required for the Proper Localization of MreB

(A) TipN-GFP localization is not affected by the addition of the MreB inhibitor, A22. A22 (10 μg/ml) was added to CJW1406 cells expressing *tipN-gfp*, and the effects of A22 on TipN-GFP were monitored in a time-course experiment. A22 had no apparent effects on TipN-GFP localization, even after 240 min of exposure when widening of the cells became visible by DIC microscopy.

(B) Proper TipN-GFP localization during the division cycle does not directly require MreB. CJW1406 cells expressing *tipN-gfp* were grown in M2G$^+$ to log-phase. A small aliquot of the culture was then mounted on an agarose-padded slide containing M2G$^+$ and A22 (2.5 μg/ml). DIC and fluorescence images were taken at regular intervals to monitor the localization of TipN-GFP and the fattening of the cells caused by the loss of MreB function. While inducing cell widening, A22 did not affect TipN-GFP relocation from the new pole to the division site at the end of the division cycle. Black and white arrows indicate stalks and TipN-GFP foci, respectively.

(C) The localization pattern of GFP-MreB is abnormal in a Δ*tipN* cell population. GFP-MreB and FtsZ-mCherry localization was examined in asynchronous cell populations of CJW1484 (wild-type *tipN*) and CJW1485 (Δ*tipN*). In the wild-type *tipN* background, GFP-MreB colocalizes with FtsZ-mCherry in a band-like pattern at the division plane of dividing cells. However, in the Δ*tipN* background, the GFP-MreB, but not the FtsZ-mCherry, band-like structure was mostly disrupted.

disrupts the MreB cytoskeleton within minutes of treatment (Gitai et al., 2005). The organization of GFP-MreB was indeed disrupted in the presence of A22 (10 μg/ml) (Figure S4A), but TipN-GFP retained its normal localization, even after 240 min of A22 exposure (Figure 5A). These observations indicated that MreB was not responsible for the maintenance of TipN at the new pole. However, they did not rule out the possibility that MreB played a role in relocating TipN to the division site at the end of the cell cycle since A22 significantly inhibits growth and cell division at a concentration of 10 μg/ml (Gitai et al., 2005) . This inhibitory effect was even more severe when A22 was present in agarose-padded slides, preventing us from doing meaningful timelapse experiments under these conditions (data not shown). To address this problem, we examined the effects of lower A22 concentrations on cell growth and GFP-MreB localization. We found that 2.5 μg/ml of A22 was sufficient to disrupt MreB localization to a level comparable to that seen with a treatment of 10 μg/ml (Figure S4B) but had the added benefit of allowing synchronous predivisional cells to fully complete at least one division (Figure 5B). Under these conditions, TipN-GFP was still able to localize to the division site where new poles were formed despite the disruption of MreB localization and accompanying cell widening (Figure 5B). We therefore concluded that the MreB cytoskeleton had no direct effect on TipN-GFP localization.

On the other hand, the loss of TipN function caused a significant effect on GFP-MreB organization. In a wild-type population, GFP-MreB exhibited a punctate subcellular distribution (46%) or a band-like localization at the division plane (54%; n = 545). This distribution of localization patterns in a mixed cell population accurately reflected the dynamic reorganization of the MreB cytoskeleton during the cell cycle (Figge et al., 2004; Gitai et al., 2004). By comparison, the band-like pattern of GFP-MreB was far less predominant (15%, n = 549) in a Δ*tipN* population (Figure S4C). It has been shown that the MreB band-like pattern is dependent on FtsZ ring formation (Figge et al., 2004). To determine whether the impaired localization of MreB in the absence of TipN was due to an indirect effect caused by defective assembly of FtsZ, we examined the localization of MreB and FtsZ in the same cells using GFP and mCherry fusions, respectively (the *ftsZ-mCherry* construct was kindly provided by M. Thanbichler, N. Hillson, and L. Shapiro). Figure 5C shows that the band-like localization of GFP-MreB was impaired in the Δ*tipN* background, even though FtsZ-mCherry formed ring-like structures.

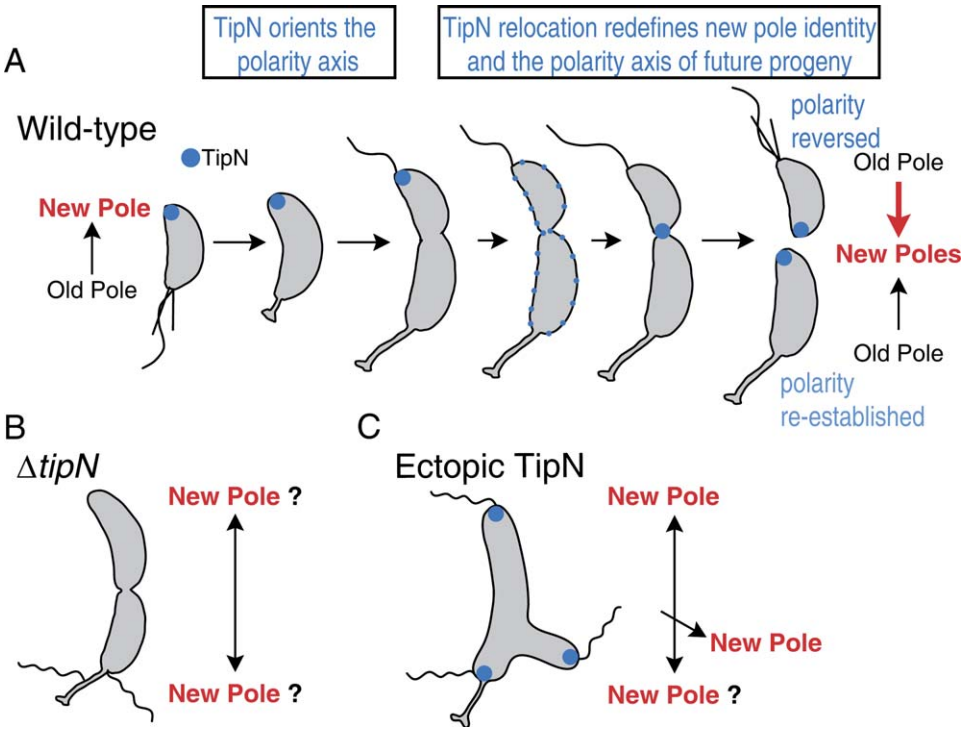

Figure 6. Model for TipN-Dependent Regulation of Cell Polarity

(A) In wild-type cells, TipN at the new pole provides a positional cue to orient and maintain the correct polarity axis, which is important for polar morphogenesis and for the correct placement of the division site. The relocation of TipN to the division site in the late predivisional cell stage redefines the identity of the poles by marking the birth site of the future progeny's new poles. Thus, TipN acts as a landmark from the previous division cycle to orient the polarity axis in the daughter cells. In the swarmer progeny, this results in a reversal of the polarity axis.

(B) In Δ*tipN* mutant cells, the landmark TipN protein is not present to identify the new pole, resulting in uncertainty about new pole identity and common misorientation of the polarity axis. Consequently, the division plane is often mispolarized toward the wrong, old pole leading to a reversed asymmetry in daughter cell size, and organelles that normally assemble at the new pole (e.g., flagellum) are often found emerging from the wrong, stalked pole or from the stalk itself.

(C) Ectopic localization of TipN at a discrete site along the lateral side of the cell identifies that site as a competent new pole, resulting in a new axis of growth and in flagellar assembly at the tip of the emerging cell branch. The presence of TipN at multiple poles including the stalked pole can also direct flagellar assembly at these sites.

Thus, TipN affects the dynamic reorganization of the MreB cytoskeleton independently of FtsZ ring formation.

DISCUSSION

In *C. crescentus*, cell polarity is readily apparent by the assembly of polar organelles and by the polarization of the division plane, which results in the generation of stalked progeny that are longer than swarmer progeny. The formation of new cell poles at division implies that cell polarity must be re-established in the stalked progeny and reversed in the swarmer progeny. Our data strongly suggest a model in which TipN regulates the orientation of the polarity axis by providing a positional cue from the preceding cell cycle. In this model (Figure 6A), TipN specifies the site of the most recent division by identifying the new pole. The cell uses this positional information as a source of intracellular asymmetry to establish and maintain the orientation of the polarity axis, which is crucial for polar morphogenesis and division. Recruitment of TipN to the nascent poles at the end of the division cycle redefines the identity of the poles and resets the correct polarity in both future daughter cells (with a polarity reversal in the swarmer cell). This critical event relies on two separable steps, each regulated independently. First, TipN delocalizes from the new pole when the cell reaches the correct size. After a brief period of fairly diffuse localization around the membrane (Figure 2B), TipN is recruited to the division site in a cell division-dependent fashion (Figures 2D and 2F). This last step provides temporal coordination between cell division and cell polarization and ensures the transmission of cell polarity to progeny cells.

Without the molecular landmark provided by TipN, cells regularly misorient their polarity axis (Figure 6B). As a result, new pole markers such as the flagellum, the CpaE pilus protein, and the PleC histidine kinase are often incorrectly targeted to the old pole (Figures 3C–3F). The accompanying paper by Huitema et al. (2006) shows that the absence of TipN also results in mistargeting of a c-di-GMP phosphodiesterase protein that is essential for flagellum

Table 1. Strains and Plasmids

Strains	Relevant Genotype or Description	Reference or Source
Caulobacter		
CJW27	CB15N (or NA1000) synchronizable variant strain of CB15	Evinger and Agabian, 1977
CJW1406	CB15N *tipN*::pBGentTtipN-gfp	This study
CJW1407	CB15N Δ*tipN*	This study
CJW1453	CB15N Δ*tipN* / pMR20tipN-gfp	This study
KR611	CB15N / pKR173	Ryan et al., 2004
CJW1449	CB15N Δ*tipN* / pKR173	This study
LS3205	CB15N *divJ*::pDivJCFP *pleC*::pPleCYFP	Wheeler and Shapiro, 1999
CJW1410	CB15N Δ*tipN divJ*::pDivJCFP *pleC*::pPleCYFP	This study
CJW1411	CB15N / pMR20tipN	This study
CJW1454	CB15N *divJ*::pDivJCFP *pleC*::pPleCYFP / pMR20tipN	This study
CJW1412	CB15N / pMR20tipN-gfp	This study
CJW1413	CB15N / pMR20PxyltipN	This study
CJW1414	CB15N / pMR20PxyltipN-gfp	This study
CJW1452	CB15N *divJ*::pDivJCFP *pleC*::pPleCYFP / pMR20PxyltipN	This study
PV418	CB15N *cpaE*::*yfp-cpaE*	Viollier et al., 2002
CJW1421	CB15N Δ*tipN cpaE*::*yfp-cpaE*	This study
LS3814	CB15N *xylX*::pXGFP4-C1mreB	Gitai et al., 2004
CJW1422	CB15N Δ*tipN xylX*::pXGFP4-C1mreB	This study
CJW1484	CB15N *xylX*::pXGFP4-C1mreB *vanA*::pNJH17	This study
CJW1485	CB15N Δ*tipN xylX*::pXGFP4-C1mreB *vanA*::pNJH17	This study
CJW1486	CB15N Δ*pleC tipN*::pBGentTtipN-gfp	This study
YB1585	CB15N *ftsZ*::pBJM1	Wang et al., 2001
CJW1487	CB15N *tipN*::pBGentTtipN-gfp *ftsZ*::pBJM1	This study
GM2471	CB15N *dnaA*::Ω *xylX*::pGM2195	Gorbatyuk and Marczynski, 2001
CJW1482	CB15N *tipN*::pBGENTtipN-GFP *dnaA*::Ω *xylX*::pGM2195	This study
CJW1423	CB15N pMR20tipN(1st Start)-GFP	This study
CJW1424	CB15N pMR20tipN(2nd Start)-GFP	This study
E. coli		
S17-1	RP4-2, *Tc*::*Mu*, *KM*-Tn*7*, for plasmid mobilization	Simon et al., 1983
DH5α	Cloning strain	Invitrogen
Plasmid	**Relevant Genotype or Description**	**Reference or Source**
pBluescriptKS+	AmpR cloning vector	Stratagene
pHL23	KanR cloning vector	This study
pMR20	TetR low-copy-number broad host range vector	Roberts et al., 1996
pMR10	KanR low-copy-number broad host range vector	Roberts et al., 1996
pBGent	GentR integration vector	Matroule et al., 2004
pEGFP	*Aequorea victoria* green fluorescent protein (GFP)	Clonetech
pBGentTtipN-gfp	pBGent carrying 5′ truncated *tipN-gfp*	This study
pKR173	pMR10 carrying *yfp-ctrA* controlled by the xylose-inducible promoter	Ryan et al., 2004
pMR20tipN	pMR20 carrying *tipN*	This study

Table 1. Continued

Strains	Relevant Genotype or Description	Reference or Source
pMR20tipN-gfp	pMR20 carrying *tipN-gfp*	This study
pMR20PxyltipN	pMR20 carrying *tipN* controlled by the xylose-inducible promoter	This study
pMR20PxyltipN-gfp	pMR20 carrying *tipN-gfp* controlled by the xylose-inducible promoter	This study
pBJM1	pBGS18T carrying the N-term portion of *ftsZ*	Wang et al., 2001
pNJH17	AprR integration vector carrying ftsZ-mcherry controlled by the vanilla-inducible promoter	M. Thanbichler, N. Hillson, and L. Shapiro
pGM2195	KanR integration plasmid carrying *dnaA* controlled by the xylose-inducible promoter	Gorbatyuk and Marczynski, 2001
pXGFP4-C1mreB	Integration vector carrying a *gfp-mreB* translational fusion under the control of the xylose-inducible promoter	Gitai et al., 2004
pET28bTtipN	pET28b His-tag vector carrying *tipN* with a 5′ truncation	This study
pMR20tipN(1st Start)-GFP	pMR20 carrying a 200 bp fragment (encompassing *tipN* promoter and TIGR-predicted leucine start codon) in a translation fusion to *gfp*	This study
pMR20tipN(2nd Start)-GFP	pMR20 carrying 800 bp fragment (encompassing *tipN* promoter, both potential start codons and 639 bp of 5′ tipN ORF) in a translational fusion to *gfp*	This study

assembly. An additional dramatic consequence of TipN loss is the frequent mispolarization of the FtsZ ring, as manifested by the reversed asymmetry in progeny size (Figures 3A and 3B). Interestingly, although TipN function is vital to the correct placement of the division site and the location of some new pole markers, it appears less important for the positioning of old pole markers such as the stalk and DivJ protein. Since the loss of TipN function results in frequently reversed cell polarity (as opposed to complete loss of polarity) for the cell division and new pole markers (Figure 3), this suggests the attractive possibility for the existence of another landmark, one that identifies the old pole. This putative old pole landmark would more specifically direct the location of old pole markers and would cause the frequent polarity reversal for TipN-dependent polarity markers seen when TipN is absent. One of the strongest lines of evidence for TipN serving as a reference point in the cell is that ectopic localization of TipN along the lateral side of the cell induces cell branching and formation of a pole functionally similar to the new pole created by division (Figure 4). The presence of TipN at an ectopic site is thus sufficient to orient a new axis of polarity at that location (Figure 6C).

TipN, originally CC1485, is annotated as a conserved hypothetical protein in the TIGR and NCBI databases. However, the sequence similarity with the proposed homologs lies mostly within the large central coiled-coil region of TipN and thus may not be relevant. On the other hand, several of these putative homologs, all in α-proteobacteria, exhibit a domain organization similar to TipN with some sequence similarity within non-coiled-coil regions. It will be of great interest to determine whether these proteins play a role in cell polarity. It is also conceivable that other coiled-coil-rich proteins may be involved in cell polarization in other bacteria. For example, in the highly polarized *Streptomyces coelicolor*, which, similar to filamentous fungi, grows as branching hyphae, the coiled-coil-rich protein $DivIVA_{SC}$ is found at the site of branch emergence and remains at the tip of extending hyphae (Flardh, 2003). While the modes of growth of *C. crescentus* and *S. coelicolor* are vastly different, it is possible that, in a manner analogous to TipN, $DivIVA_{SC}$ acts as a landmark for the establishment and maintenance of new axes of polarity necessary for hyphal growth in *S. coelicolor* (Flardh, 2003).

In eukaryotic cells such as yeast, development of intrinsic cell polarity follows a stereotypical hierarchy of events (Drubin and Nelson, 1996). First, an intrinsic spatial cue originating from the preceding division determines the cell polarity site. This site is then recognized by landmark proteins, which act as a reference point in the cell to recruit and organize signaling proteins. This signaling complex then polarizes the actin cytoskeleton to propagate the positional information into the interior of the cell. Our data strongly suggest that the prokaryote *C. crescentus* also uses a landmark protein (TipN) associated with the previous division site to establish the correct polarity in the progeny. The actin homolog MreB is thought to play an analogous role to that of actin in eukaryotic cells by mediating cell polarization in *C. crescentus* (Gitai et al., 2004). We show that TipN affects the dynamic organization of the MreB cytoskeleton whereas MreB does not appear to directly control TipN localization (Figure 5), suggesting

that TipN is upstream of MreB in regulating cell polarity. This suggests that the underlying mechanisms involved in cell polarization are similar between eukaryotic and prokaryotic cells. With the principle of the eukaryotic hierarchy in mind, we propose that TipN recruits or organizes signaling proteins at the new pole. This polarized complex would then transduce the positional information to the MreB cytoskeleton, which, in turn, would propagate cell polarization inside the cell and regulate the placement of the FtsZ division ring and the location of new pole markers such as the flagellum. The characterization of TipN-interacting partners may therefore unravel general signaling mechanisms by which bacterial cells can achieve and perpetuate cell polarity.

EXPERIMENTAL PROCEDURES

Strains, Plasmids, Media, and Growth Conditions

C. crescentus strains were grown at 30°C in PYE (peptone yeast extract) or M2G supplemented with 1% PYE ($M2G^+$). Plasmids were mobilized from *E. coli* strain S17-1 into *C. crescentus* by bacterial conjugation (Ely, 1991). Plasmids and strains are listed in Table 1 and the strategies for their construction are available upon request. Synchronous cell populations were obtained as described (Evinger and Agabian, 1977). Cultures in mid-log phase were used for all described experiments. Swarm assays were performed in 0.3% agar as described (Burton et al., 1997). Since the *tipN* gene may be organized in an operon with *wbqP* (Awram and Smit, 2001; Nierman et al., 2001), a gene required for lipopolysaccharide O-antigen synthesis, we generated an in-frame deletion of *tipN* (Δ*tipN*; CJW1407) to avoid a possible polar effect on downstream expression of *wbqP*. Western blot analysis using anti-O-antigen antibodies confirmed that the O-antigen, and thus WbqP function, was normal in Δ*tipN* cells (data not shown). Expression of *yfp-ctrA* (KR611, CJW1449) or expression of *gfp-mreB* (LS3814, CJW1422, CJW1484, CJW1485) were achieved by addition of 0.3% or 0.03% xylose for 2 hr as described (Gitai et al., 2004; Ryan et al., 2002). Expression of *ftsZ-mcherry* (CJW1484, CJW1485) was attained by addition of 0.5 mM vanillic acid for 2 hr, whereas induction and repression of *ftsZ* (YB1585, CJW1487) and *dnaA* (GM2471, CJW1482) were achieved by addition of 0.3% xylose and 0.3% glucose, respectively. Overexpression of *tipN-gfp* in CJW1414 was achieved by addition of 0.3% xylose for 18 hr. Of note, overexpression of untagged *tipN* (CJW1413) generates a more severe branching phenotype than *tipN-gfp* under similar inducing conditions (data not shown), suggesting that the GFP-tagged protein is not 100% functional. However, as described above, chromosomal replacement of *tipN* by *tipN-gfp* under endogenous expression does not lead to any apparent motility or morphological defects, indicating TipN-GFP was by and large functional.

Identification of TipN

We used the COILS algorithm (Lupas, 1996) to identify highly coiled-coil-rich proteins in the *C. crescentus* genome (P. Obuchowski, H.L., and C. J.-W, unpublished data). A subsequent search for candidates that contained membrane spanning regions (Tusnady and Simon, 1998, 2001) reduced our list of proteins to a few candidates, which included *CC1485*, now renamed *tipN*.

The original, proposed start of the *CC1485* (*tipN*) open reading frame was at the chromosomal position of 1639877, starting with a leucine codon (Nierman et al., 2001). However, when a 440 bp fragment encompassing the *tipN* promoter up to this leucine codon was fused to *gfp* to produce a translational fusion (strain CJW1423), no GFP was produced whereas a larger fragment containing a methionine codon 15 nucleotides downstream resulted in *gfp* expression (data not shown) (strain CJW1424). In light of these results, we propose that the *tipN* coding sequence begins at this methionine codon at the chromosomal position of 1639895.

Preparation of TipN Antibodies and Immunoblotting Experiments

N-terminally polyhistine-tagged TipN lacking the first 238 N-terminal residues was expressed from the pET-28b vector (Novagen, CA) in *E. coli* BL21 (DE3) and purified using BD TALON Metal Affinity Resin (BD Biosciences Clontech, CA) under denaturing conditions (6 M urea) as described in the user manual. Purified His-tagged protein was used as an antigen to generate antibodies in rabbits (Proteintech Group, IL). Immunoblot analysis was performed using α-TipN (1/20,000), α-O-antigen (1/300,000) (Awram and Smit, 2001), α-GFP JL-8 (Clontech, CA; 1/1000), α-CtrA (1/10,000), and α-MreB (1/20,000).

Microscopy and Statistical Analysis

For electron microscopy imaging, cells grown in PYE were spotted on glow-discharged carbon-coated grids, stained with 1% uranyl acetate for 1 min, and imaged on a Zeiss EM10C transmission electron microscope (80kV).

For light microscopy imaging, cell populations of *C. crescentus* strains were placed on an agarose-padded slide containing $M2G^+$ (Jacobs et al., 1999). Samples were observed at room temperature (~22°C) on a Nikon E1000 microscope through a 100× DIC objective using a Hamamatsu Orca-ER LCD camera. Images were taken and processed with Metamorph software (Universal Imaging, PA). For the cell size measurements, cells in length greater than 4 μm with no apparent division-plane constriction or cells >5 μm in length were deemed elongated. To determine the bias of the division plane location in wild-type and Δ*tipN* cells, DIC images of late predivisional cells were analyzed. A multiline tool (Metamorph) was used to draw the shortest curved line between each pole and the division plane in each cell. The length of the resulting line was then used to determine the ratio between the lengths of the stalked and swarmer cell compartments. To identify the length of CJW1406, CJW1487, and CJW1482 cells at the time of TipN-GFP delocalization, timelapse experiments were performed and DIC images of cells were measured (as described above) at the time of corresponding TipN-GFP delocalization.

Flagellar Staining

Cells were grown to mid-log phase in PYE and immediately fixed with a solution containing paraformaldehyde and $NaPO_4$ (pH 7.5) to final concentrations of 2.5% and 30 mM, respectively. After 30 min of incubation at room temperature (RT), the samples were incubated with DAPI stain (1.5 μg/ml) for another 15 min at RT. The cells were mounted and imaged as described above, using a UV filter. For presentation in Figures 3, 4, and 5, the images were processed using the Metamorph "Sharpening" function to enhance the visualization of the flagella. Using this DAPI staining technique, we could detect a flagellum in 33% and 13% of mixed populations of wild-type and Δ*tipN* cells, respectively, suggesting that TipN may play a role in flagellum synthesis or maintenance, in addition to its role in flagellum placement.

Supplemental Data

Supplemental data include four figures and three movies and can be found with this article online at http://www.cell.com/cgi/content/full/124/5/1011/DC1/.

ACKNOWLEDGMENTS

We thank Waldemar Vollmer for critical reading of this manuscript and a collaboration on TipN not presented here; Martin Thanbichler, Nathan Hillson, and Lucy Shapiro for allowing us to use the Pvan-FtsZ-mCherry construct prior to its publication; Patrick Viollier, Kathleen Ryan, Greg Marczynski, Yves Brun, Jim Gober, John Smit, and Zemer Gitai for supplying us with strains and antibodies; Barry Piekos for assistance with the EM; David Kysela for help with database searches; and the

Jacobs-Wagner laboratory for critical reading of this manuscript and general friendship. This work was supported by National Institutes of Health grant GM065835 and the Pew Scholars Program in the Biological Sciences sponsored by the Pew Charitable trust (to C.J.-W.).

Received: August 23, 2005
Revised: November 10, 2005
Accepted: December 6, 2005
Published: March 9, 2006

REFERENCES

Awram, P., and Smit, J. (2001). Identification of lipopolysaccharide O antigen synthesis genes required for attachment of the S-layer of Caulobacter crescentus. Microbiol. *147*, 1451–1460.

Burton, G.J., Hecht, G.B., and Newton, A. (1997). Roles of the histidine protein kinase pleC in Caulobacter crescentus motility and chemotaxis. J. Bacteriol. *179*, 5849–5853.

Chant, J., and Pringle, J.R. (1995). Patterns of bud-site selection in the yeast Saccharomyces cerevisiae. J. Cell Biol. *129*, 751–765.

Domian, I.J., Quon, K.C., and Shapiro, L. (1997). Cell type-specific phosphorylation and proteolysis of a transcriptional regulator controls the G1-to-S transition in a bacterial cell cycle. Cell *90*, 415–424.

Drubin, D.G., and Nelson, W.J. (1996). Origins of cell polarity. Cell *84*, 335–344.

Ely, B. (1991). Genetics of Caulobacter crescentus. Methods Enzymol. *204*, 372–384.

Evinger, M., and Agabian, N. (1977). Envelope-associated nucleoid from Caulobacter crescentus stalked and swarmer cells. J. Bacteriol. *132*, 294–301.

Figge, R.M., Divakaruni, A.V., and Gober, J.W. (2004). MreB, the cell shape-determining bacterial actin homologue, co-ordinates cell wall morphogenesis in Caulobacter crescentus. Mol. Microbiol. *51*, 1321–1332.

Flardh, K. (2003). Essential role of DivIVA in polar growth and morphogenesis in Streptomyces coelicolor A3(2). Mol. Microbiol. *49*, 1523–1536.

Gitai, Z., Dye, N., and Shapiro, L. (2004). An actin-like gene can determine cell polarity in bacteria. Proc. Natl. Acad. Sci. USA *101*, 8643–8648.

Gitai, Z., Dye, N.A., Reisenauer, A., Wachi, M., and Shapiro, L. (2005). MreB actin-mediated segregation of a specific region of a bacterial chromosome. Cell *120*, 329–341.

Gorbatyuk, B., and Marczynski, G.T. (2001). Physiological consequences of blocked Caulobacter crescentus dnaA expression, an essential DNA replication gene. Mol. Microbiol. *40*, 485–497.

Huitema, E., Pritchard, S., Matteson, D., Radhakrishnan, S.K., and Viollier, P.H. (2006). Bacterial birth scar proteins mark future flagellum assembly site. Cell *124*, this issue, 1025–1037.

Jacobs, C., Domian, I.J., Maddock, J.R., and Shapiro, L. (1999). Cell cycle-dependent polar localization of an essential bacterial histidine kinase that controls DNA replication and cell division. Cell *97*, 111–120.

Judd, E.M., Ryan, K.R., Moerner, W.E., Shapiro, L., and McAdams, H.H. (2003). Fluorescence bleaching reveals asymmetric compartment formation prior to cell division in Caulobacter. Proc. Natl. Acad. Sci. USA *100*, 8235–8240.

Lupas, A. (1996). Prediction and analysis of coiled-coil structures. Methods Enzymol. *266*, 513–525.

Matroule, J.Y., Lam, H., Burnette, D.T., and Jacobs-Wagner, C. (2004). Cytokinesis monitoring during development; rapid pole-to-pole shuttling of a signaling protein by localized kinase and phosphatase in *Caulobacter*. Cell *118*, 579–590.

Nierman, W.C., Feldblyum, T.V., Laub, M.T., Paulsen, I.T., Nelson, K.E., Eisen, J.A., Heidelberg, J.F., Alley, M.R., Ohta, N., Maddock, J.R., et al. (2001). Complete genome sequence of Caulobacter crescentus. Proc. Natl. Acad. Sci. USA *98*, 4136–4141.

Nilsen, T., Yan, A.W., Gale, G., and Goldberg, M.B. (2005). Presence of multiple sites containing polar material in spherical Escherichia coli cells that lack MreB. J. Bacteriol. *187*, 6187–6196.

Ohta, N., and Newton, A. (1996). Signal transduction in the cell cycle regulation of Caulobacter differentiation. Trends Microbiol. *4*, 326–332.

Roberts, R.C., Toochinda, C., Avedissian, M., Baldini, R.L., Gomes, S.L., and Shapiro, L. (1996). Identification of a *Caulobacter crescentus* operon encoding *hrcA*, involved in negatively regulating heat-inducible transcription, and the chaperone gene *grpE*. J. Bacteriol. *178*, 1829–1841.

Ryan, K.R., Judd, E.M., and Shapiro, L. (2002). The CtrA response regulator essential for Caulobacter crescentus cell-cycle progression requires a bipartite degradation signal for temporally controlled proteolysis. J. Mol. Biol. *324*, 443–455.

Ryan, K.R., Huntwork, S., and Shapiro, L. (2004). Recruitment of a cytoplasmic response regulator to the cell pole is linked to its cell cycle-regulated proteolysis. Proc. Natl. Acad. Sci. USA *101*, 7415–7420.

Shih, Y.L., Kawagishi, I., and Rothfield, L. (2005). The MreB and Min cytoskeletal-like systems play independent roles in prokaryotic polar differentiation. Mol. Microbiol. *58*, 917–928.

Simon, R., Prieffer, U., and Puhler, A. (1983). A broad host range mobilization system for in vivo genetic engineering: transposon mutagenesis in gram-negative bacteria. Biotechnology (N. Y.) *1*, 784–790.

Terrana, B., and Newton, A. (1975). Pattern of unequal cell division and development in Caulobacter crescentus. Dev. Biol. *44*, 380–385.

Tusnady, G.E., and Simon, I. (1998). Principles governing amino acid composition of integral membrane proteins: application to topology prediction. J. Mol. Biol. *283*, 489–506.

Tusnady, G.E., and Simon, I. (2001). The HMMTOP transmembrane topology prediction server. Bioinformatics *17*, 849–850.

Viollier, P.H., Sternheim, N., and Shapiro, L. (2002). A dynamically localized histidine kinase controls the asymmetric distribution of polar pili proteins. EMBO J. *21*, 4420–4428.

Wagner, J.K., Galvani, C.D., and Brun, Y.V. (2005). Caulobacter crescentus requires RodA and MreB for stalk synthesis and prevention of ectopic pole formation. J. Bacteriol. *187*, 544–553.

Wang, Y., Jones, B.D., and Brun, Y.V. (2001). A set of *ftsZ* mutants blocked at different stages of cell division in Caulobacter. Mol. Microbiol. *40*, 347–360.

Wheeler, R.T., and Shapiro, L. (1999). Differential localization of two histidine kinases controlling bacterial cell differentiation. Mol. Cell *4*, 683–694.